

Variational Shape Approximation of Point Set Surfaces

Martin Skrodzki^{a,*}, Eric Zimmermann^b, Konrad Polthier^b

^a*ICERM, Brown University, Providence, RI, USA*

and RIKEN iTHEMS, Wako, Saitama, Japan

^b*Freie Universität Berlin, Berlin, Germany*

Abstract

In this work, we present a translation of the complete pipeline for variational shape approximation (VSA) to the setting of point sets. First, we describe an explicit example for the theoretically known non-convergence of the currently available VSA approaches. The example motivates us to introduce an alternate version of VSA based on a *switch* operation for which we prove convergence. Second, we discuss how two operations—*split* and *merge*—can be included in a fully automatic pipeline that is in turn independent of the placement and number of initial seeds. Third and finally, we present two approaches how to obtain a simplified mesh from the output of the VSA procedure. This simplification is either based on simple plane intersection or based on a variational optimization problem. Several qualitative and quantitative results prove the relevance of our approach.

Keywords: Variational Shape Approximation, Point Set Segmentation, Simplification

2010 MSC: 68U05, 68U07, 65D18

1. Introduction

Point sets arise naturally in almost all kinds of three-dimensional acquisition processes, like 3D laser-scanning. As early as 1985, they have been recognized as fundamental shape representations in computer graphics by Levoy and Whitted (1985). Ever since, they have found manifold applications e.g. in face recognition, traffic accident analysis, archaeology, and several other fields.

*Corresponding author: mail@ms-math-computer.science

However, in many applications, large parts of the point set carry redundant information. For example, a flat area of a surface can be sampled sparsely without—compared to an area of high curvature—losing information. In several applications, it is not even necessary to consider all details carried by the point set. For instance, in architecture—for a first draft—the rough outline of a building suffices and there is no need to send more detailed geometries. In general, when transmitting geometries e.g. to give an overview of a certain portfolio, the general outlines of the geometries suffices and sending only these saves on bandwidths during transmission. In this sense, algorithms are necessary that reduce a complex geometry to several basic shapes that still retain the most important features of the input. Towards this end, Cohen-Steiner et al. (2004) proposed their *Variational Shape Approximation* (VSA) for meshes.

The VSA procedure segments a mesh into a given number of flat proxy regions, see Section 3. Finally, a simplified surface is obtained with only one element for each region, see Section 5. A translation of the VSA method to the setting of point sets was done by Lee and Bo (2016) with the explicit goal of feature curve extraction. While VSA is able to provide an easy to implement simplification of any geometry, it also has several downsides. First, it is dependent on the number of proxies which has to be chosen a priori. Second, in the previous publications, the quality of the result depends heavily on the manual placement of the starting seeds for the proxies (Cohen-Steiner et al. (2004); Lee and Bo (2016); Yan et al. (2006)). Towards this end, two manual operations were proposed, which allow for splitting proxy regions of high error and merging neighboring ones with a combined low error (Cohen-Steiner et al., 2004, Sec. 3.5). In the context of meshes, these operations have been automatized (Yan et al., 2006, Sec. 3.1). Third and finally, the previous publications were not able to construct a VSA algorithm with guaranteed convergence. This article closes these gaps. Our main contributions are:

- Providing an example of a growing error during the run of the VSA algorithm which applies to meshes and point sets alike.
- Presentation of a modified VSA procedure including the *switch* operation and proof of its guaranteed convergence.
- Inclusion of the two operations, *split* and *merge*, as automatic parts in the point set processing pipeline, making the initial choice of a fixed proxy number and the manual selection of seeds unnecessary.

- Extension of variational tangent plane intersection to the setting of point sets and inclusion of the procedure in the VSA pipeline for simplification.

This paper is an extension of a chapter in a PhD thesis (Skrodzki, 2019, Chapter 5). Some results of the paper have been presented as a poster at the International Geometry Summit 2019 in Vancouver, Canada and have been published in the corresponding poster proceedings, see Skrodzki et al. (2019).

2. Related Work

The VSA procedure was introduced by Cohen-Steiner et al. (2004) as a method for concise, faithful approximation of complex three-dimensional meshes. It does so by fitting a set of planar proxies to the input mesh. We will provide a detailed discussion of the procedure in Section 3. As the resulting elements are oriented corresponding to all associated faces of the original mesh, the effects of simplification are less drastic as in the classical approach of Garland and Heckbert (1997). A next step towards even better approximations consisted of the inclusion of more than just planar shapes. In the work of Wu and Kobbelt (2005), also e.g. cylinders and spheres are used as proxies to even better approximate the input shape. This was generalized even further by Yan et al. (2006) who utilized general quadrics as proxies to be fitted to the input. However, all these methods are implemented in the setting of surface meshes.

A translation of the VSA procedure to the setting of point sets was performed in an article by Lee and Bo (2016). The authors studied the problem of computing smooth feature curves from CAD type point cloud models. Their reconstructed curves arise from the intersections of developable strip pairs which approximate the regions along both sides of the features. The generation of the developable surfaces is in turn based on VSA. While the presented results are convincing, it remains unclear whether the approach of fitting developable surfaces works outside of the CAD realm. Furthermore, the work does not provide details on how to obtain the used linear planar approximations or how to construct a watertight mesh from them. These aspects motivate the present research.

Our proposed approach incorporates two different areas of point set processing. On the one hand, we aim at segmenting the input into several flat—i.e. planar—parts. Thus, we will discuss related segmentation approaches

in Section 2.1. On the other hand, we want to construct a simplified mesh on the basis of the found flat surfaces patches. Therefore, we will present corresponding work on mesh generation and simplification in Section 2.2.

2.1. Segmentation

Segmentation of point clouds is the process of classifying the input into multiple homogeneous regions, where points in the same region will have the same properties. In real-world applications—like intelligent vehicles, autonomous mapping, and navigation—the problem is challenging because of high redundancy, uneven sampling density, and lack of explicit structure in the input data. Methods for point set segmentation can roughly be classified as follows: edge-based, region-based (seeded/bottom-up or unseeded/top-down), attribute-based, model-based, graph-based, or machine-learning-based, see Nguyen and Le (2013), Grilli et al. (2017). Following this terminology, the VSA procedure is a seeded, region-based method, which is characterized by starting the segmentation process from seed points and letting regions grow by adding neighbors if they satisfy certain conditions—like normal similarity. We refer to the survey of Nguyen and Le (2013) for a discussion of several corresponding methods. In this work, the authors draw the following conclusion on seeded region-based methods:

[They] are highly dependent on selected seed points. Inaccurate choosing seed points will affect the segmentation process and can cause under or over segmentation.

The survey paper of Grilli et al. (2017) draws a similar conclusion for the corresponding set of discussed methods. Hence, in contrast to the procedures covered in the mentioned surveys, we put an emphasis on the independence of both the number and placement of seed points. See Section 4.3 for a corresponding discussion.

Point cloud segmentation can be considered either from a semantic or from a geometrical perspective. The former aims at separating a model into its parts: A chair should for instance be segmented into four legs, a seating surface, and a backrest. The geometric approach is to segment the model into different primitives as well as possible. A recent survey paper of Xie et al. (2019) provides a comprehensive list of methods following both approaches. In the terminology used in this paper, the VSA approach creates a “plane point cloud segmentation”. While we cannot discuss all works mentioned, we

will consider two popular approaches in the following and refer to the survey of Xie et al. (2019) for a thorough discussion of other related work.

Note that fitting different planar segments to a model can be considered as a natural approach in order to render the model with a reduced set of planar patches. Naturally, those models are captured well that are comprised of mostly planar surface parts. The presence of spherical or cylindrical shapes will cause for larger distortions when approximating only with planar parts. Thus, a next step—after planar fitting—is the usage of other geometric primitives, like spheres, cylinders, cones, or tori. Each of these primitives then require their own fitting. As the VSA approach only fits planes, we briefly discuss different fitting concepts for this primitive. Note at this point that the method of Wu and Kobbelt (2005) utilizes the exact same procedure for fitting of planes as the original VSA paper by Cohen-Steiner et al. (2004).

To fit a planar patch, the approach of Schnabel et al. (2007) considers three points $p_i, p_j, p_\ell \in P$ from an input point set P and computes a normal of the plane spanned by these points. This normal is then compared to the respective normals at p_i, p_j , and p_ℓ . A fitting plane is introduced if all three normal variations stay below a user-given angle. Clearly, the results of this approach heavily depends on the choice of the three points.

In contrast, the approach of Attene and Patanè (2010) places a plane at the weighted barycenter b of a considered subset $\{p_i\} \subset P$ of the input point set P . A weighted covariance matrix is used to determine a normal n and the fitting error is computed as a weighted least-squares formulation. However, this computation neglects the normal information at the points p_i .

Another choice for the segmentation of point clouds is the algorithm of Rabbani et al. (2006). It is popular because of its easily accessible implementation in the widely used Point Cloud Library (PCL) by Rusu and Cousins (2011). This method can be seen as a reduced version of the VSA approach. Regions are also grown from seeds according to normal information. However, the growing process is only executed once and not repeated from a different set of seeds, like in VSA (see Section 3). Thus, the result is even more dependent on the initial seeding than in other, comparable techniques.

For the give reasons, the discussed methods have their respective downsides. Contrasting the presented algorithms, in our translation of the VSA approach, we include the entire normal information of the input point set. Furthermore, we have a setup of the pipeline that ensures independence of the initial seed points, which eliminates the major disadvantage of seed-based region growing methods.

2.2. Meshing and Simplification

As stated in Section 1, the ultimate goal of our VSA procedure for point sets is to create a simplified mesh from a set of planar proxy regions. That is, a set of mesh vertices has to be created from the intersection of the proxy planes. Then, these vertices have to be connected to represent face elements for the proxies respectively. While three pairwise non-parallel planes intersect in a unique point, this is not necessarily the case for more than three planes in \mathbb{R}^3 . In the context of planar panelization of freeform surfaces, Zimmer et al. (2012) confirm this statement, asserting that tangent plane intersection is numerically not stable enough to obtain reliable results. The authors proceed to present a variational approach and a corresponding minimization problem in order to obtain a planar representation of a given mesh structure. This method improves the approach of Cutler and Whiting (2007) for constrained planar remeshing of architectural geometries, which is itself based on VSA. Therefore, we turn to the work of Zimmer et al. (2012) to make the calculation of a simplified mesh from the input point set as robust as possible. See Section 5 for a discussion of the technical details of the optimization and also for our translation to the setting of point sets.

Aside from VSA, there are other approaches to obtain a simplified mesh from an input point set. For instance, a possibility is to first mesh the input point set and then simplify the created mesh. An overview of methods for meshing of point sets is presented in the survey of Berger et al. (2017). Several methods are available for the subsequent simplification of the mesh. These mostly collapse edges in the mesh to reduce its complexity. By using quadric error metrics, it can be assured that the collapses remove elements that carry the least amount of feature information, see Garland and Heckbert (1997). This simple approach can be improved by adjusting the position of the vertex resulting from an edge collapse according to the local curvature information, see Hua et al. (2015); Yao et al. (2015). However, as these methods perform their operations in a greedy manner, they do not provide reliable results when performing a drastic number of simplifications. Also, these approaches require a costly meshing operation on the unfiltered point set, which can introduce topological failures, like a surface of wrong genus or flipped triangles.

Another possibility to obtain a simplified mesh from an input point set is to first simplify the point set and to then create a mesh from this. A brief introduction and (error) analysis of different point set simplification algorithms can be found in the work of Pauly et al. (2002). Important at-

tributes in real-world applications are the performance and quality of the rendering process. This requires a specific focus on features represented by the point sets. By utilizing a bilateral filtering, both Euclidean distances and normal information can be taken into account throughout a simplification process on a point set to best preserve both the large-scale geometry and small-scale features, in Sosorbaram et al. (2010). While these methods are feature-preserving, they are not robust in the presence of outliers or noise. Also, the construction of the mesh cannot use the full information of the input point set anymore, as the majority of points will have been removed during the simplification step.

Because of the downsides of both the approaches, we aim at taking all points of the input into account when creating planar proxies. From these, we then create a mesh by completely creating new vertices and connections on them without going through a costly meshing operation on the original input, see Section 5.

3. The Method

In this section, we will present the Variational Shape Approximation (VSA) as introduced by Cohen-Steiner et al. (2004) and as used by Yan et al. (2006) for surfaces and surface meshes. Also, we present a translation of the procedure to the setting of point sets, similar to the work of Lee and Bo (2016).

3.1. The VSA Procedure for Surfaces and Surface Meshes

The VSA procedure of Cohen-Steiner et al. (2004) acts on a surface $S \subseteq \mathbb{R}^3$. The goal is to partition S into m disjoint regions $R_i \subseteq S$, $\bigcup R_i = S$, where each region is associated a linear proxy (C_i, N_i) with a center $C_i \in \mathbb{R}^3$ and a unit-length normal $N_i \in \mathbb{R}^3$, $i \in \{1, \dots, m\}$. The authors propose two different metrics to find the optimal shape proxies, with the first metric based on the \mathcal{L}^2 measure

$$\mathcal{L}^2(R_i, C_i, N_i) = \int_{x \in R_i} \|x - \pi_i(x)\|_2^2 dx, \quad (1)$$

where $\pi_i(\cdot)$ denotes the orthogonal projection of the argument on the plane with normal N_i centered at C_i . Thus, the integral (1) measures the squared error between points in the region R_i and its linear approximation given by (C_i, N_i) .

A second metric, denoted by $\mathcal{L}^{2,1}$ is based on the \mathcal{L}^2 measure when evaluated on the normal field. It is given by

$$\mathcal{L}^{2,1}(R_i, N_i) = \int_{x \in R_i} \|n(x) - N_i\|_2^2 dx, \quad (2)$$

where $n(x)$ denotes the normal of the surface at point $x \in S$. As Cohen-Steiner et al. (2004) conclude that the $\mathcal{L}^{2,1}$ metric is more effective, we will reduce the following discussion to this formulation.

In the discrete setting, the surface S is given by a finite set of $T \in \mathbb{N}$ (triangular) elements t_j , $j \in [T]$ and the centers C_i are found by randomly choosing a triangle t_j as center C_i . Therefore, the second smooth formulation (2) can be discretized to

$$\mathcal{L}^{2,1}(R_i, N_i) = \sum_{t_j \in R_i} \|n(t_j) - N_i\|_2^2 \cdot |t_j|, \quad (3)$$

with $n(t_j)$ the normal and $|t_j|$ the area of the element t_j respectively.

The actual minimization of expression (3) with respect to the segmentation of S into regions R_i and with respect to the proxies (C_i, N_i) is then performed iteratively. For this, a variation of Lloyd’s fixed point iteration given by Lloyd (1982) is used. The first step is to pick a user-given number m of center elements C_1, \dots, C_m randomly from the set of triangles $\{t_j \mid j \in [T]\}$. The normals N_i are set to the normals of corresponding center triangles C_i and the regions are initialized as $R_i = \{t_i\}$. The neighbors of the chosen center triangles are collected in a priority queue \mathcal{Q} sorted increasingly with growing $\mathcal{L}^{2,1}$ -distance between neighboring triangle and center triangle: $\|n(t_j) - N_i\|_2^2$. Then, the following three steps are performed iteratively until convergence:

1. *Flood*: As long as the queue \mathcal{Q} is not empty, pop the first element t_j from \mathcal{Q} . Ignore it, if it has already been assigned to a region. If it is not assigned yet, assign it to the region R_i that pushed it into the queue and push all neighboring elements of t_j into \mathcal{Q} , noting that they have been pushed by R_i . Without loss of generality, we assume S to be connected. If that is not the case, the algorithm can simply be run on each connected component of S . For a connected surface S , after the queue \mathcal{Q} has been emptied, all elements $\{t_j \mid j \in [T]\}$ have been assigned to some region respectively.

2. *Proxy Update*: The proxy normals N_i are updated according to

$$N_i = \frac{\sum_{t_j \in R_i} |t_j| n(t_j)}{\left\| \sum_{t_j \in R_i} |t_j| n(t_j) \right\|_2},$$

where it is ensured that the updated N_i are unit-length normals. Note that as the surface will be segmented into a large enough number of locally flat patches, the denominator of this expression will never be zero in practice.

3. *Seed*: For each region R_i , find some element $t' \in R_i$ such that

$$\|n(t') - N_i\|_2^2 \leq \|n(t_j) - N_i\|_2^2$$

for all $t_j \in R_i$. This ensures that the flooding in the next iteration is started from regions that best reflect the current proxy normals.

Finally, the iteration is stopped, when no region changes from one step to the next. From the converged regions R_i and assigned proxies (C_i, N_i) , a simplified mesh with corresponding m surface elements is constructed. Respective results are shown in Cohen-Steiner et al. (2004).

3.2. The VSA Procedure on Point Sets

We will now proceed to present a translation of the VSA procedure to the setting of point sets. A corresponding reformulation can be found in Lee and Bo (2016), while we include weights to obtain a more general setup. Compared to the VSA on meshes, several details have to be adjusted for the method to work on point sets. At first, consider the partition problem as stated in Section 3.1. In the context of point sets, not elements, but the points themselves have to be assigned to the proxies. That is, the given point set $P = \{p_1, \dots, p_N\}$ will be partitioned into disjoint subsets $\bigcup_{i=1}^m P_i = P$, $m \in \mathbb{N}$. Therefore, in the following expressions, the centers C_i denote points from the point set P , while the normals N_i at the respective center point are those obtained from a normal field imposed on the point set. The normals of the points $p_j \in P$ will be denoted by n_j respectively.

Consider the energy as defined in Equation (3). For proxies obtained from point sets, the area term $|t_j|$ cannot be used. Thus, we replace it by a weighting term $\omega_j \in \mathbb{R}_{\geq 0}$ which is to approximate the area represented by

the point $p_j \in P$. We obtain the following energy of a single proxy and the resulting energy formulation on the set of all proxies

$$\mathcal{L}^{2,1}(P_i, N_i) = \sum_{p_j \in P_i} \omega_j \|n_j - N_i\|_2^2, \quad (4)$$

$$E(\{(P_i, N_i) \mid i = 1, \dots, m\}) = \sum_{i=1}^m \mathcal{L}^{2,1}(P_i, N_i). \quad (5)$$

An approximation of the area term can be obtained by

$$\omega_j = \sum_{\ell \in \mathcal{N}(j)} \|p_\ell - p_j\|_2^2, \quad (6)$$

where $\mathcal{N}(j) \subset P$ denotes the neighborhood of p_j in P . Including weights reflecting the area are of interest because of varying densities. Therefore, another possible weighting scheme could be the incorporation of directional density measures proposed in Skrodzki et al. (2018). This could be coupled in a bilateral manner together with the Euclidean distances mentioned before. In contrast, weight determination via normal deviations should not be used, as the energy is defined upon these, i.e. weighting these terms in the same fashion seems counterproductive.

The initial seeding as outlined above can still be done in the point cloud setting, but instead of triangles, now, $m \in \mathbb{N}$ points $p_j \in P$ are chosen for the initial position of the center points C_i . Also, those points from P are pushed to the priority queue \mathcal{Q} that are neighbors, but not identical, to the chosen center points C_i . For this neighborhood relation, any neighborhood concept such as combinatorial k -nearest neighborhoods or geometric neighborhoods of radius r can be used. Denote the neighborhood of p_i by $\mathcal{N}(i) \subset P$. Again, the points in \mathcal{Q} are sorted increasingly with \mathcal{L}^2 distance between their own normal and the normal of the proxy that pushed them into the queue: $\|n_j - N_i\|_2^2$. The following three iteratively applied steps remain almost unchanged:

1. *Flood*: As long as the queue \mathcal{Q} is not empty, pop the first element p from \mathcal{Q} . Ignore it, if it has already been assigned to a subset P_i . If it is not assigned yet, assign it to the subset P_i that pushed it into the list and push all neighboring points $p_j \in \mathcal{N}(i)$ into \mathcal{Q} , noting that they have been pushed by P_i . As we assume S to be connected via the imposed neighborhood relation (see above), after the queue \mathcal{Q} has been emptied, all elements of P have been assigned to some subset P_i .

2. *Proxy Update*: The proxy normals N_i are updated according to

$$N_i = \frac{\sum_{p_j \in P_i} \omega_j n_j}{\left\| \sum_{p_j \in P_i} \omega_j n_j \right\|_2},$$

where we once again obtain unit-length normals and will not encounter a denominator equal to zero (see above).

3. *Seed*: For all subsets P_i , find some $p_\ell \in P_i$, $\ell \in [\mathbb{N}]$, such that

$$\|n_\ell - N_i\|_2^2 \leq \|n_j - N_i\|_2^2$$

for all $p_j \in P_i$. Again, this ensures that the next flooding step starts from regions that best reflect the current proxy normals.

Finally, once the subsets P_i do not change anymore over two iterations, the process is stopped. From the converged subsets P_i and assigned proxies (C_i, N_i) , a simplified mesh with corresponding m surface elements is constructed. Respective results are shown in Lee and Bo (2016), while our corresponding approach will be discussed in Section 5.

4. Improved VSA Pipeline

Having described the VSA procedure for both meshes and point sets in the previous chapter, we now turn to our contributions for this pipeline. First, we will establish by an example that convergence of neither the meshed nor the point set version is guaranteed. Following up on this, we propose an alternative formulation of VSA with guaranteed convergence. Furthermore, we turn to a different issue of the VSA procedure. Namely, it is highly depended on both the number of initial seeds and their placement at the beginning of the procedure. We circumvent this dependency by including two more operations in the point set pipeline that have already been used manually Cohen-Steiner et al. (2004) and automatically Yan et al. (2006) in the context of meshes.

4.1. Example for Failure of Convergence of the VSA Procedure

Concerning the convergence of their algorithm, Cohen-Steiner et al. (2004) state:

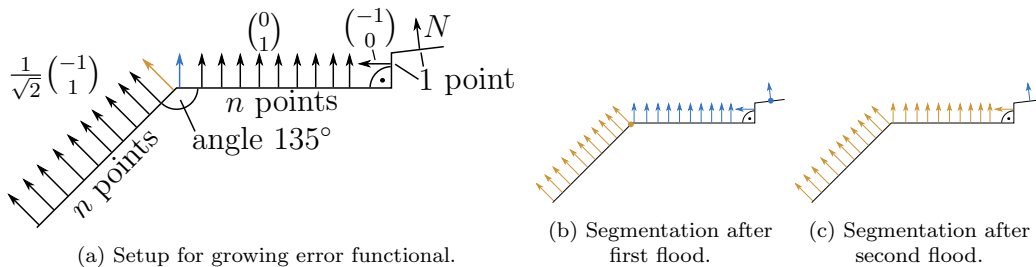


Figure 1: Example for a growth in the error measure after a flood and proxy update.

[...] *Lloyd's algorithm always converges in a finite number of steps, since each step reduces the energy E : the partitioning stage minimizes E for a fixed set of centers c_i , while the fitting stage minimizes E for a fixed partition.*

While this statement holds for the original algorithm of Lloyd as presented in Lloyd (1982), it does not hold for neither the VSA procedure on meshes as presented in Cohen-Steiner et al. (2004); Yan et al. (2006) nor for the translation to point sets as given by Lee and Bo (2016). This is already recognized in the paragraph *Convergence* of Section 3.5 in Cohen-Steiner et al. (2004). We will demonstrate this with the following concrete example, which is to the best of our knowledge the first explicit example presented.

Consider the two-dimensional setup shown in Figure 1a. It is given by n points connected on a line with normal $\frac{1}{\sqrt{2}}\begin{pmatrix} -1 \\ 1 \end{pmatrix}$ next to a line of n points with normal $\begin{pmatrix} 0 \\ 1 \end{pmatrix}$. At the right end of the second line, there is a single point with normal $\begin{pmatrix} -1 \\ 0 \end{pmatrix}$ and another single point with normal N given by the equation

$$N = \frac{1}{\|n \cdot \begin{pmatrix} 0 \\ 1 \end{pmatrix} + \begin{pmatrix} -1 \\ 0 \end{pmatrix} + N\|_2} \cdot \left(n \cdot \begin{pmatrix} 0 \\ 1 \end{pmatrix} + \begin{pmatrix} -1 \\ 0 \end{pmatrix} + N \right),$$

which solves to $N = \frac{1}{\sqrt{n^2+1}}\begin{pmatrix} -1 \\ n \end{pmatrix}$. Now, two proxies will act on this example, with their initial seeds shown in yellow and blue in Figure 1a. They each start on one of the two lines of n points respectively. The result after a flood is shown in Figure 1b, where each line is completely covered by the proxy starting on it and the two single points are associated to the proxy with normal $\begin{pmatrix} 0 \\ 1 \end{pmatrix}$. After updating the proxy normals, the yellow proxy has normal $\frac{1}{\sqrt{2}}\begin{pmatrix} -1 \\ 1 \end{pmatrix}$ while the blue proxy has normal N given by the equation above. Thus, the yellow proxy starts from an arbitrary point on its line

while the blue proxy starts from the rightmost point. The error after this first flood and proxy update is given by

$$E_1 = n \cdot \left\| \begin{pmatrix} 0 \\ 1 \end{pmatrix} - N \right\|_2^2 + \left\| \begin{pmatrix} -1 \\ 0 \end{pmatrix} - N \right\|_2^2 = -2(\sqrt{n^2 + 1} - n - 1),$$

where only the blue proxy contributes to the error, because the normals corresponding to the yellow proxy coincide with their proxy normal and cancel out in energy E_1 . Starting from the new seed points, a second flood results in the situation shown in Figure 1c. Here, almost all points except for the rightmost one are associated to the yellow proxy with former normal $\frac{1}{\sqrt{2}} \begin{pmatrix} -1 \\ 1 \end{pmatrix}$. Its new normal after a proxy update is

$$N' = \frac{1}{\left\| \frac{n}{\sqrt{2}} \cdot \begin{pmatrix} -1 \\ 1 \end{pmatrix} + n \cdot \begin{pmatrix} 0 \\ 1 \end{pmatrix} + \begin{pmatrix} -1 \\ 0 \end{pmatrix} \right\|} \cdot \left(\frac{n}{\sqrt{2}} \cdot \begin{pmatrix} -1 \\ 1 \end{pmatrix} + n \cdot \begin{pmatrix} 0 \\ 1 \end{pmatrix} + \begin{pmatrix} -1 \\ 0 \end{pmatrix} \right),$$

which amounts to an error after the second flood and proxy update given by

$$E_2 = n \cdot \left\| \frac{1}{\sqrt{2}} \begin{pmatrix} -1 \\ 1 \end{pmatrix} - N' \right\|_2^2 + n \cdot \left\| \begin{pmatrix} 0 \\ 1 \end{pmatrix} - N' \right\|_2^2 + \left\| \begin{pmatrix} -1 \\ 0 \end{pmatrix} - N' \right\|_2^2.$$

Note that the error term for the blue proxy cancels out, as the one representative corresponds to the normal of the proxy it belongs to. Choosing $n = 100$ points on each of the two lines, we obtain $E_1 \approx 1.9900$, but $E_2 \approx 31.6782$. Furthermore, the corresponding error value after the flood is also growing. Thus, convergence cannot be proven by an always shrinking error functional.

Note that this example is described as a curve in 2D, where neighborhood selection is generally more involved than for surfaces in 3D. However, the example can easily be extended to a surface in 3D space, see Figure 2. There, we also close the loop and thereby cause the original VSA algorithm to run infinitely long. For the given example, the crucial step as depicted in Figure 1c can be resolved via a manual (Cohen-Steiner et al. (2004)) or automatic (Yan et al. (2006)) split of the large proxy. Thus, this example only applies to the VSA procedure as described above.

4.2. VSA with guaranteed Convergence

The example presented above highlights the main deficiency of the VSA procedure as used in Cohen-Steiner et al. (2004); Yan et al. (2006); Lee and Bo (2016). Namely, if an outlier causes a proxy normal to be distorted,

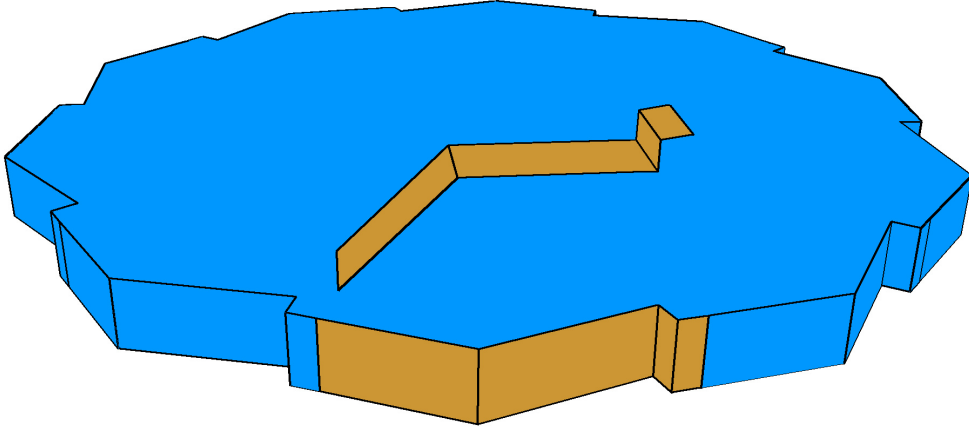


Figure 2: A regular 10-gon, built from the shape shown floating on top, which is a three-dimensional extension of the setup shown in Figure 1a.

the new proxy seed can end up to be a border point that does not actually reflect the normal behavior of the majority of points in the proxy. In other words, the change of seeds before flooding is a problematic step. Thus, in the following, we aim at altering the VSA procedure in a way such that no new seeds need to be found, but proxies can still move and alter. In particular, proxies should be able to take over the original seed points of other proxies if necessary. These changes should finally lead to an alternative VSA procedure with guaranteed convergence. In order to achieve this goal, we propose to alter the steps of the algorithm as follows.

First, we perform an initial seeding and one flood step and proxy update as explained in Sections 3.1 and 3.2 above. Instead of the seeding step in the following iterations, we perform a different procedure:

4. *Switch*: Consider the neighborhoods $\mathcal{N}(i) \subset P$ for all points $p_i \in P$. Assume that p_i is assigned to subset P_ℓ . If any point $p_j \in \mathcal{N}(i)$ is assigned to another subset P_h , compute the change of the error measure (5) resulting from reassigning p_i from P_ℓ to P_h . Compare it to the current best known reassignment. After iterating through all points $p \in P$, reassign the point such that the error measure is reduced

maximally.

This new switch step replaces the *seed* step and the *flood* step described in Sections 3.1 and 3.2 above. That is, it is only iterated together with the *proxy update*. The iteration is continued until no further switch operations can be performed. For this alternate procedure, we can prove the following statement.

Theorem 1 (Error reduction by switch and proxy update). *Given a point set $P = \{p_1, \dots, p_n\}$ with a neighborhood structure, such that the neighborhood graph on P is connected and normals n_1, \dots, n_n on P . Then, each proxy update step and each switch step as defined above leads to proxies (P_i, C_i, N_i) with a smaller error measure in Equation (5).*

Proof. Concerning the proxy update step, consider

$$\begin{aligned} \nabla E(\{(P_i, N_i) \mid i \in [m]\}) &= \nabla \sum_{i=1}^m \mathcal{L}^{2,1}(P_i, N_i) \\ &= \sum_{i=1}^m \sum_{p_j \in P_i} \nabla \omega_j \|n_j - N_i\|_2^2 \\ &= \sum_{i=1}^m \sum_{p_j \in P_i} 2\omega_j (n_j - N_i). \end{aligned}$$

Setting $N_i = \frac{\sum_{p_\ell \in P_i} \omega_\ell n_\ell}{\sum_{p_\ell \in P_i} \omega_\ell}$, we obtain

$$\begin{aligned} \sum_{p_j \in P_i} 2\omega_j (n_j - N_i) &= \sum_{p_j \in P_i} 2\omega_j n_j - \sum_{p_j \in P_i} 2\omega_j \left(\frac{\sum_{p_\ell \in P_i} \omega_\ell n_\ell}{\sum_{p_\ell \in P_i} \omega_\ell} \right) \\ &= \sum_{p_j \in P_i} 2\omega_j n_j - \left(\frac{\sum_{p_\ell \in P_i} 2\omega_\ell n_\ell}{\sum_{p_\ell \in P_i} \omega_\ell} \right) \cdot \sum_{p_j \in P_i} \omega_j \\ &= \sum_{p_j \in P_i} 2\omega_j n_j - \sum_{p_\ell \in P_i} 2\omega_\ell n_\ell = 0. \end{aligned}$$

Thus, at the chosen updated proxy normal, the energy reaches a (local) minimum. As the energy is convex as sum of norms, which are convex, the found minimum is indeed its global minimum for the current choice of segmentation.

Concerning the switch step, only those points are reassigned which reduce the value of error measure (5). Thus, trivially, after a switch operation the error is smaller. \square

Finally, we note that there are only finitely many ways to partition the \aleph points of the point set P into m subsets. This fact, together with Theorem 1 proves the convergence of our modified VSA procedure.

Consider the application of this alternative VSA version to the setup in Figure 1a. After a first flood, which would still result in the proxies shown in Figure 1b, the only possible switch could be performed at the border between the blue and the yellow region. However, a switch would already lead to an increase of the energy functional. Thus, the proxies remain as they are after the first flood and the example converges immediately.

By replacing *seed* and *flood* with the *switch* operation, we can ensure convergence of the algorithm. While this result is theoretically pleasing, it is not necessarily of practical value. Finding an ideal pair of points for a switch operation requires to iterate at least over all points on the border of proxy regions. Depending on the number of proxies and on the shape of the geometry, one such switch can reach the same time complexity as a flood operation while only altering a single point's proxy assignment. Thus, in practice, utilizing the *switch* operation causes a significantly longer runtime as trade-off to the guaranteed convergence.

Furthermore, iterated application of the switch operation can tear a proxy apart, see Figure 3. A converged state of the algorithm might therefore include proxy regions that are not connected. In order to have a sensible result, a final step has to be included that re-interprets connected regions as proxies and that might increase the number of proxies doing so. However, a disconnectedness only arises if another proxy better reflects the local shape. Thus, a corresponding higher number of connected proxy regions is desirable in order to faithfully approximate the input geometry.

The presented *switch* operation provides one possible way to obtain guaranteed convergence. It remains an open question whether another operation or alteration of the VSA procedure provides the same result while coming with a lower runtime.

4.3. User controlled Level of Detail

The requirements of proper seed placement and prescribed seed number naturally demand for a variable proxy-treatment in terms of *splits* and *merges*.

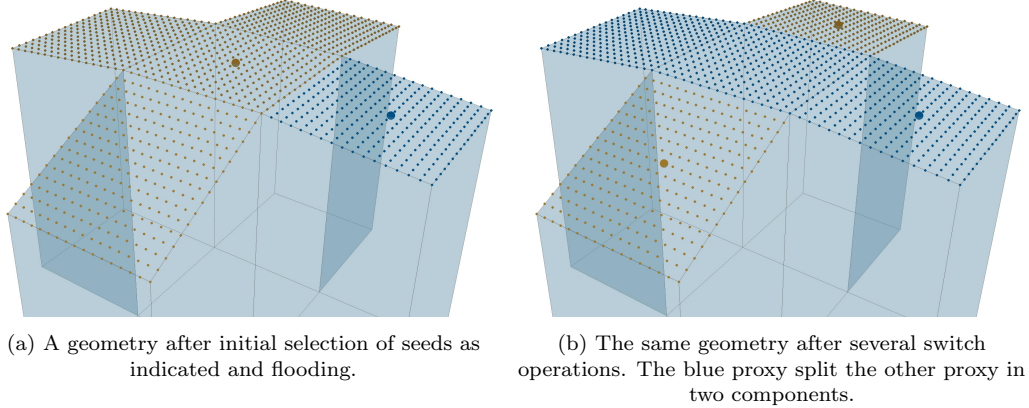


Figure 3: A proxy being torn apart by another proxy under the repeated application of the switch operation.

Both concepts were introduced in Cohen-Steiner et al. (2004) as means for manual adjustments by the user. For meshes, these two operations are incorporated into the pipeline described in Yan et al. (2006). In the following, we propose a translation to point sets. With both operations, we aim at adaptability of the constructed flat pieces towards user input. That is, the user should be able to control the level of detail obtained from the flat regions. However, in contrast to Cohen-Steiner et al. (2004), this control should be realized via a single input parameter instead of a time-consuming manual interaction with the modeling process. For this, we use a user-given parameter $\eta \in \mathbb{R}_{\geq 0}$ which controls the maximum deviation of a subset P_i from its flat approximation. It can be thought of as controlling the maximum bending of a segment. This parameter is used in the following two steps:

- (a) *Split*: Given a subset $P_i \subset P$ such that $\mathcal{L}^{2,1}(P_i, N_i) > \eta$. We use weighted principal component analysis by Harris et al. (2011) to compute the most spread direction of P_i . The set P_i is then split at the center of this direction into two new sets $P_i = P_i^1 \dot{\cup} P_i^2$. The new normals are chosen as $N_i^1 = \sum_{p_j \in P_i^1} \frac{\omega_j n_j}{\sum_{p_j \in P_i^1} \omega_j}$ and N_i^2 respectively. The new centers C_i^1 and C_i^2 are then placed at those points of P_i^1 and P_i^2 that have least varying normals from N_i^1 and N_i^2 respectively.

Note that the reasoning of Theorem 1 holds for this case, too. Thus, the procedure outlined above, with an additional split step does continue

to converge.

- (b) *Merge*: Consider a pair P_i, P_j of neighboring subset with their respective normals N_i, N_j . If the subset $P' = P_i \cup P_j$ with normal

$$N' = \left\| \frac{|P_i| \cdot N_i + |P_j| N_j}{|P_i| + |P_j|} \right\|^{-1} \frac{|P_i| \cdot N_i + |P_j| N_j}{|P_i| + |P_j|}$$

achieves an Energy (5) strictly less than η , the two subsets are replaced by their union P' , with normal N' and a chosen center $C' \in P'$ with its normal least deviating from N' .

Note that we could allow only those pairs of neighboring regions to merge such that

$$\mathcal{L}^{2,1}(P_i, N_i) + \mathcal{L}^{2,1}(P_j, N_j) \geq \mathcal{L}^{2,1}(P', N').$$

Then, the energy would not increase and termination of the algorithm would be guaranteed by Theorem 1. However, this would result in neighboring regions not observing the user-given η threshold. Therefore, we accept an increase of the global energy in favor of a better region layout¹.

Both operations alter the number m of proxies. Thereby, a significant disadvantage of the algorithm of Lloyd (1982) is eliminated as the user does not have to choose m a priori. It is replaced by the user's choice of η , providing a semantic guarantee on the regions being built by the algorithm. The user can prescribe a value of η based on the curvature and number of points within a proxy. See Appendix A for a more detailed interpretation of η .

The possible presence of noise in the point set P gives yet another reason to refute Energy (1). For points distributed around the xy -plane, with normals $(0, 0, 1)^T$ and just slight deviation from the plane, this energy would create larger values for a growing number of points, while the Energy (5) does not suffer from this. Hence, with the chosen energy, noise on the point positions is handled more robustly.

¹Note that the equation for N' in this description of the *merge* procedure deviates from the equation given in the published version of the article in *Computer Aided Geometric Design 2020, Vol. 80*. The formulation given here is more general and works in particular if P_i and P_j are of different sizes. Furthermore, in the published version, the inequality on $\mathcal{L}^{2,1}$ was given in the wrong direction, which is corrected here.

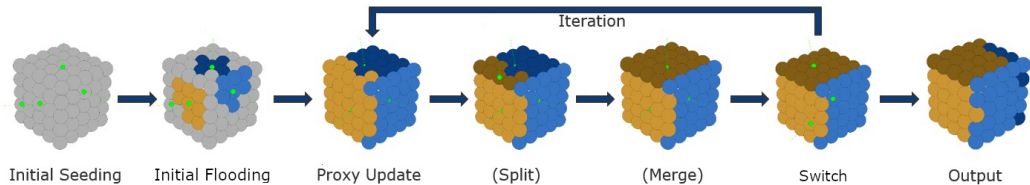


Figure 4: The whole pipeline contains an initial random seed selection and an initial flooding. From there, a proxy update, one or more optional splits and/or merges, and a switch are iterated until no further switches can be applied. Afterwards, we deduce a simplified model according to the proxies, which can also be considered as a simplified surface reconstruction from the initial point set.

In the merge process outlined above, we asked for two neighboring regions. However, we have not defined any relation on the regions yet. In the meshed case discussed in Section 3.1, two regions are neighbors if and only if they share an edge in the mesh. In the context of point sets, we cannot rely on this, thus we have used the following approach. For every proxy and each of its points, we query k of the point’s nearest neighbors and use the distance to the farthest of them for a geometric neighborhood determination. From all the neighbors gathered that way, we ask for their proxy assignment. If the current center point is assigned to a different proxy than its neighbors, we consider the two proxies to be neighbors. This finishes the whole pipeline, including the additional two steps *merge* and *split*. See Figure 4 for an illustration of the complete pipeline.

5. Simplification

We will now investigate the creation of a simplified mesh based on the segmentation generated before. Both works of Cohen-Steiner et al. (2004) and Lee and Bo (2016) present simplified meshed geometries with m faces, one representing each proxy. The work of Yan et al. (2006) also presents simplified meshes, utilizing their proxy quadrics. However, the approaches of Cohen-Steiner et al. (2004) and Yan et al. (2006) are not suitable for our context as they work on meshes. The authors of Lee and Bo (2016) do not elaborate on the computation of their meshes. They only state that

(...) a polygonal mesh is easily generated by computing intersections of proxy planes of neighboring clusters of data points.

In the following, we will see that only simple cases allow for this approach while the general case is more involved. First, we will discuss the creation of vertices for the simplified mesh (Section 5.1). Subsequently, we will connect these vertices to faces in order to obtain the complete mesh (Section 5.2). In both sections we also address corresponding challenges as well as possible solutions.

5.1. Vertices for a Simplified Mesh

The intuitive way to determine simplified mesh vertices is the intersection of neighboring proxies, as used by Lee and Bo (2016). In the following, we will use the notion of neighborhood for proxies as introduced at the end of Section 4.3.

Intersecting Planes. A first naive solution for the creation of vertices for the simplified mesh is to consider the intersection of neighboring proxies and the construction of vertices in these intersection points. In the general case, where $q > 3$ proxy planes meet, we cannot simply consider the intersection as it will be mostly empty.

We call such a situation obtained via the proxy-neighborhood relation an q -tuple. In detail, let I be the index set labeling the proxies given by subset $P_i \subseteq P$, proxy center C_i , and proxy normal N_i . Further, consider all neighborhood relations $(i, j) \in I \times I$ between proxies. A q -tuple is a subset $\{i_1, \dots, i_q\}$ of I such that the proxies i_j and i_ℓ are neighbors for all $i_j, i_\ell \in \{i_1, \dots, i_q\}$ where $i_j \neq i_\ell$. Enumerate all such q -tuples I_j by an index set J in a way, s.t. if there are $j, j' \in J$ with $I_j \subsetneq I_{j'}$, then the larger set $I_{j'}$ is kept and j is not stored in J . These tuples hold inclusion maximal candidates for intersection points with proxy indices contributing to the intersection.

Now, for the case of $q > 3$, we select for each tuple three indices at random, intersect them, and make the resulting vertex known to all proxy members of the tuple. As this might cause degenerate faces in the face creation stage—as the vertex does not lie within all of the proxies it is associated to—we use a triangulation of all created faces (see Section 5.2) to obtain triangles, which are planar.

Intersecting Point Optimization. A second, more involved solution for the creation of simplified mesh vertices is based on optimization. The intersection of more than three planes is numerically unstable as discussed above. In the

work of Zimmer et al. (2012), the authors turn to a variational approach, start from a triangle mesh, and aim at computing the intersection points x_j of the vertex tangent planes of all triangles. Thus, exactly three tangent planes—corresponding to each of the three vertices v_i of a triangle—contribute to an intersection point. Denoting the normal at v_i by n_i , they solve the following minimization problem

$$\begin{aligned} \text{minimize: } & \sum_{t_j} \left(\sum_{v_i \in t_j} \|x_j - v_i\|_2^2 \right) \\ \text{subject to: } & n_i^T(v_i - x_j) = 0 \quad \forall t_j, \quad \forall v_i \in t_j \\ & \|n_i\|_2^2 = 1 \quad \forall v_i \end{aligned} \tag{7}$$

where the normals are variables in the minimization. Note that the original normals at the vertices are not taken into account at all during the minimization. The requirement of unit-length normals is necessary, however, as otherwise $n_i = 0$ would trivially satisfy all conditions.

We generalize this approach in the following way to our setup. First of all, we use the concept of and notation for q -tuples introduced in the previous paragraph. Then, we consider the following energy

$$F(\{x_1, \dots, x_j\}) = \sum_{j \in J} \left(\sum_{i \in I_j} \|x_j - C_i\|_2^2 \right) + \sum_{i \in I} \tilde{w}_i \|N_i - \tilde{n}_i\|_2^2, \tag{8}$$

with sought-for intersection points x_j for each maximal tuple I_j , known proxy-centers C_i , weighting terms $\tilde{w}_i \in \mathbb{R}_{\geq 0}$, unknown normal deviations \tilde{n}_i , and known proxy-normals N_i for all proxies $i \in I$. Ultimately, we want to solve

$$\begin{aligned} \text{minimize: } & F(\{x_1, \dots, x_j\}) \\ \text{subject to: } & \tilde{n}_i^T(x_j - C_i) = 0 \quad \forall j \in J \quad \forall i \in I_j \\ & \|\tilde{n}_i\|_2^2 = 1 \quad \forall i \in I. \end{aligned} \tag{9}$$

This generalizes the problem of Zimmer et al. (2012) as stated in Equation (7) in several ways. First, we allow for more than three, namely for an arbitrary number of planes to intersect. This arises already at a simple geometry like the octahedron, which has valence 4 vertices, see Figure 5a for an illustration. Second, we do allow the normals \tilde{n}_i to deviate from the proxy normals N_i ,

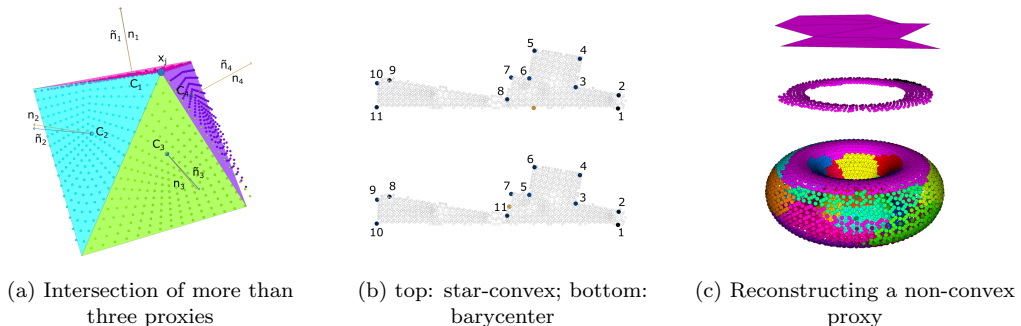


Figure 5: (a) Illustration of point optimization with deviation allowance (represented by \tilde{n}_i) of n_1, \dots, n_4 to find the optimal mesh vertex x_j satisfying the constraints $\langle C_i - x_j, \tilde{n}_i \rangle = 0$ and $\|\tilde{n}_i\|_2^2 = 1$ for $i = 1, \dots, 4$. The C_i are the normal-corresponding proxy-centers and n_i the original proxy normals. (b) Star-convex proxy (front part of the fandisk, Figure 9). Top shows an ordering of the vertices around a star-convex center point, bottom shows the corresponding ordering around the barycenter. (c) Bottom: Segmentation of the Torus with 24 final proxies. Middle: Non-convex proxy representing the upper part of the torus after projection of the points onto their proxy plane. Top: Resulting mesh face after connecting the vertices.

but a large deviation is punished, where the severity can be steered by the weights \tilde{w}_i .

In contrast to the first naive solution, this approach guarantees all vertices of the mesh to lie within the proxies that they are derived from. That is, if the optimization problem (9) yields a feasible point, after correcting the proxy normals from n_i to \tilde{n}_i all vertices associated to a planar proxy lie completely within the corrected proxy plane.

5.2. Faces for a Simplified Mesh

After creating the mesh vertices, we need to connect them in order to generate face for the mesh. The general idea is to represent every proxy region with a single star-convex face. All vertices associated to a proxy are sorted around the barycenter of the proxy w.r.t. an arbitrary reference direction. This yields correct results, when the barycenter of the proxy is also a star-convex center point, see Figure 5b. If we sort the vertices with a non-star-convex center, they are connected in wrong order and the resulting faces will degenerate. This approach obviously fails, if a proxy represents a non-convex part of the geometry, see Figure 5c.

6. Experimental Results

The following experimental section is divided into two parts. First, we evaluate parameter choices regarding the segmentation and provide a quantitative comparison of the segmentation results. In the second part, we discuss three aspects of the simplification algorithm on clean and noisy models.

In all our experiments, we processed models with quite uniform samplings. Hence, for simplicity, we utilized equal weights $\omega_j = 1$ in Equation (4). We proceed similarly with the weight assignment in the optimization problem formulated in Equation (8) and set $\tilde{w} = 1$. We use neighborhoods to both propagate a proxy during the *flood* step and establish neighborhood relations between the different proxies. For the first purpose, we use a combinatorial k -nearest neighbors approach. When determining the proxy neighborhoods, we turn to a combination of the combinatorial and geometric approach based on the same k (see end of Section 4.3). In all our experiments, we use $k = 8$. Deviations from the default parameters are indicated.

6.1. Segmentation

For a large scale experiment, we chose 600 models from the repository used in the work Hu et al. (2018). For all these models, we used the mesh information to generate an oriented vertex normal field. Furthermore, we translated the models and scaled them uniformly to fit into the unit cube. Finally, we performed our experiments on the point cloud given by the mesh vertices, disregarding the connectivity information and the triangular faces.

We compared four different approaches. The first one was the segmentation algorithm of Rabbani et al. (2006) as implemented in the *Point Cloud Library* of Rusu and Cousins (2011). As parameters, we turned to the ones described in the original paper, see Rabbani et al. (2006). We will refer to this experiment by *PCL*. Second, with these results at hand, we took the final numbers of proxies given by *PCL* for each geometry. This number served as number of proxies to be sought by the variational shape approximation algorithm of Lee and Bo (2016). Here, no splits or merges are applied, thus we refer to this experiment by $\neg s/m$. Third, we took the total $\mathcal{L}^{2,1}$ -error (Equation (5)) of each geometry, as produced by the *PCL* experiment, and divided it by its final number of proxies. This division provides an initial guess for a local, geometry-dependent value η . In this third experiment, we allowed splits as well as merges. Also, we started with an initial seed number of $m = \aleph$, i.e. each point was a seed at the start. Because of the η -threshold

and merge-processes, the number of proxies reduced drastically over the run of the experiment. We will refer to this as *local* η s/m . Fourth and finally, without any priors, we set $\eta = 25$ and allowed splits and merges. Furthermore, we once more started with every point as a seed. The choice of η is motivated from previous experiments. We will refer to this fourth experiment as *global* η s/m . The terminology *local* or *global* indicates whether η is chosen with respect to the geometry or globally for all geometries. Observe that the experiments $\neg s/m$ and *local* η s/m are dependent on the results of *PCL*, while only *global* η s/m is independent.

We are interested in gaining insight into the relationship between the obtained proxy-number m and the quality of the induced flat proxy-regions. Besides the $\mathcal{L}^{2,1}$ -measure of Equation 5, we focus on the mean squared error (MSE) caused by point-to-proxy-plane distances to evaluate the region quality. The MSE is given as

$$MSE(\{(P_i, N_i) \mid i = 1, \dots, m\}) = \frac{1}{\aleph} \sum_{p_j \in P_i} \|p_j - \pi(p_j)\|_2^2, \quad (10)$$

where $\pi(p_j)$ denotes the orthogonal projection of p_j onto its related proxy plane, given by normal N_i and base point C_i .

From the 600 chosen models, we obtained 499 that offered segmentation results in all four experiments. For 27 models, *PCL* was unable to provide a valid segmentation, because it assigned a zero proxy-normal to at least one region (for instance a region holding only two antipodal normals). These models were excluded for the subsequent experiments. The variational shape segmentation of Lee and Bo (2016) did not report a complete segmentation on additional 72 models. Here, some points are not assigned to any proxies, because they cannot be reached from the proxy centers during a *flood* when traversing the nearest neighbor graph. Increasing the parameter k alleviates this problem. Similar failures occurred on one additional model in experiments *local* η s/m and *global* η s/m respectively. Even though these experiments started with seed numbers equal to the geometries' points, they reduced the number of regions via *merge* operations. Due to proxy updates and new seed selection, it is possible that seeds travel away from sparsely sampled areas, where they do not reach all formerly assigned points in the neighborhood graph during the next *flood*. This reduced the number of models by a total of 101 failures to 499 feasible models. All reported experimental values are taken over this set of 499 models.

	<i>PCL</i>	$\neg s/m$	<i>local $\eta s/m$</i>	<i>global $\eta s/m$</i>
min MSE	2.75E-09	7.31E-07	6.95E-11	2.11E-06
max MSE	1.12E-01	2.98E-02	4.15E-02	1.04E-02
avg MSE	1.59E-02	2.88E-04	6.40E-04	4.50E-04
sd MSE	2.12E-02	1.90E-03	2.47E-03	8.15E-04
min m	1.00	1.00	2.00	1.00
max m	1,103.00	1,103.00	393.00	135.00
avg m	174.17	174.17	55.05	33.20
sd m	163.10	163.10	58.41	20.69

Table 1: Statistical evaluation of error MSE and proxy number m taken over all 499 geometries. We give the minimum, maximum, mean, and standard deviation.

For the following analysis, we turn to Table 1. There, we give statistics on both the MSE as obtained from experiments on our model set. Regarding the average MSE over all experiments, we see that all three experiments— $\neg s/m$, *local $\eta s/m$* , and *global $\eta s/m$* —outperform *PCL* by two orders of magnitude. A direct comparison between the MSE obtained for the models reveals that *local $\eta s/m$* and *global $\eta s/m$* outperform $\neg s/m$ in roughly 8.5% of all experiments. Note that the minimal MSE error obtained over all geometries is up to five orders of magnitude smaller for *local $\eta s/m$* when compared with the other experimental setups.

Aside from the MSE results, Table 1 also reports statistics on the number of proxies obtained by the different experiments over all geometries. Recall that we are not only interested in small error values, but also in representations of the geometry that reduce its complexity, i.e. that have a low number of proxies. Towards this end, it is remarkable that *local $\eta s/m$* and *global $\eta s/m$* attain MSE values comparable to those of $\neg s/m$ while only using 31.6% and 19.1% of the proxies on average, respectively. The close error results are especially of interest for *global $\eta s/m$* , as this runs without any dependency or information provided by *PCL*, as a global parameter is applied to all geometries equally. Hence, the assignment of points to proxies is on one hand optimized in terms of the MSE errors measure, while providing significantly fewer proxies on the other hand. Note that the lowest (and therefore optimal) MSE of 0 is given for a segmentation in which every point is represented by its own proxy.

We proceed to further investigate the proxies obtained by the different

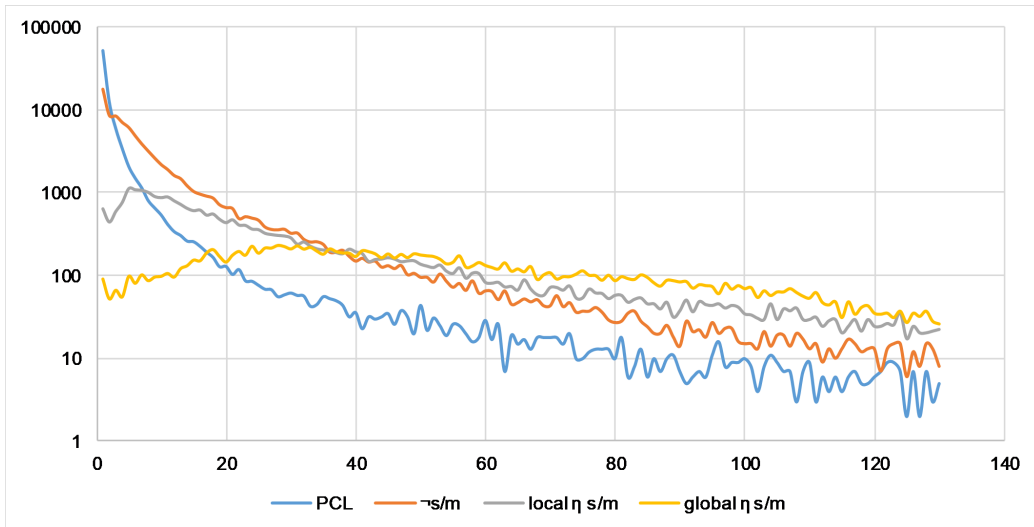


Figure 6: Histogram over all proxy-sizes up to 131 among all 499 geometries for all four experiments. The upper bound of 131 is given by the sum of the mean (11.74) and corresponding standard deviation (120.27) regarding cluster sizes obtained from *PCL*. Note the logarithmic scale on the y -axis.

experiments. In Figure 6, we show a histogram over the attained proxy-sizes taken over all geometries in the experiment. Note that the y -axis has a logarithmic scale. We show all proxy sizes up to 131, where this bound is given by the sum of the mean (11.74) and corresponding standard deviation (120.27) regarding proxy sizes obtained from *PCL*. We can see that both *PCL* and $\neg s/m$ create a significantly larger number of small proxies when compared with the segmentation results of *local $\eta s/m$* and *global $\eta s/m$* . In fact the average proxy sizes are 11.74 (*PCL*, $\neg s/m$), 37.15 (*local $\eta s/m$*), and 64.00 (*global $\eta s/m$*). As segmentation—in our setup—should create few regions that still reflect the geometry attributes, extremely small regions as exposed by *PCL* and $\neg s/m$ are undesirable. The availability of splits and merges in *local $\eta s/m$* and *global $\eta s/m$* results in a bell-curve-like behavior in Figure 6, as both curves first increase and show a small descent with minor oscillations after their peaks. Hence, in the critical area of small sized proxies, the availability of splits and merges not only reduces their required number, but also balances their sizes, causing for more uniformly sized proxies.

To summarize the quantitative analysis of the segmentation part, we conclude:

- The proposed method outperforms the segmentation approach of Rabbani et al. (2006) as well as variational shape approximation without splits and merges, as used by Lee and Bo (2016) in regard of MSE.
- Without any knowledge of seed numbers or error values, a globally set η , availability of splits as well as merges, and treatment of all points as initial seeds provides segmentation results that have MSE comparable to Rabbani et al. (2006); Lee and Bo (2016) but a significantly reduced number of proxies.
- The availability of splits and merges not only optimizes for small proxy numbers, but also causes more uniform region sizes.

6.2. Simplification

In the following, we present different experiments regarding the simplification as obtained from the proxy segmentation. Each experiment addresses different aspects of the simplification pipeline. First, we consider how the parameter η influences the obtained simplification (Section 6.2.1). Next, we turn to the Fandisk model, to discuss difficulties arising due to face generation (Section 6.2.2). The last experiment deals with a noisy geometry and robustness of our algorithm (Section 6.2.3).

Throughout our experiments, in order to solve the minimization problem (9), we turn to the build-in solver of Matlab. Note that the minimization problem has a non-linear target function with non-linear constraints and can thus not be solved by any LP or even ILP solver. Hence, we follow the example from the Matlab manual Mathworks and Matlab, which is supported by all versions newer than *R2019b*. The solver asks for starting points from which to run the optimization. We initialize the normals \tilde{n}_i by the proxy normals N_i . As first guesses for any intersection point x_j , we chose the barycenter of the centers C_i of those proxies that contribute to this intersection.

6.2.1. Threshold η -dependency on the Sphere Model

Our first simplification model is a sphere sampled with $\aleph = 5,122$ points. We chose this model as it also appears in Cohen-Steiner et al. (2004); Lee and Bo (2016). By running our algorithm with 12 initial centers without split and merge we obtain a segmentation into 12 planar faces, shown together

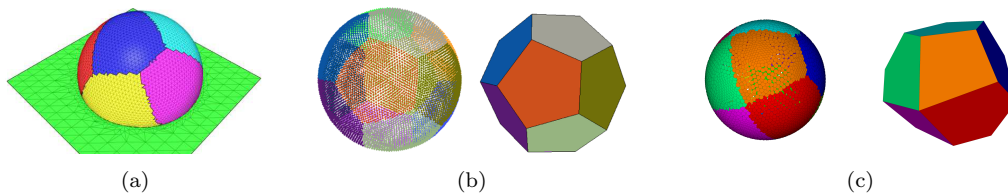


Figure 7: A visual comparison of the output of (a) Cohen-Steiner et al. (2004) showing a segmentation of the half-sphere into six proxies, (b) Lee and Bo (2016) with a segmentation of the sphere into 12 proxies, and (c) the results of our algorithm applied to the sphere deducing 12 proxies.

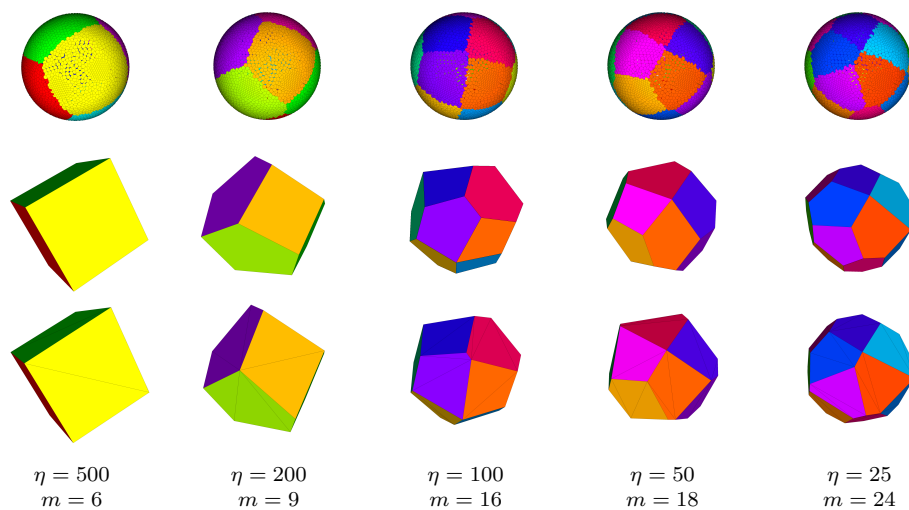


Figure 8: The segmentation and simplification for different η values. The first row shows the segmented point sets, the second and third rows the meshes deduced via optimization and plane intersection, respectively.

with the simplification done by optimization in Figure 7 coupled with results of Cohen-Steiner et al. (2004); Lee and Bo (2016).

In Figure 8, we show segmentation and simplification results w.r.t. different values of η taken from $\{500, 200, 100, 50, 25\}$. The utilized geometry is the sphere used above. The simplification points are calculated via both approaches introduced in Section 5, i.e. via intersection of the proxy planes and via the optimization problem given in Equation (9). All results are obtained from the same set of six randomly selected seed points. For the optimization case $\eta = 500$ we increased the weight $\tilde{w}_i = 3$, as otherwise the simplification points would have produced a smaller version of the cube. Hence, in this case we forced the optimization putting more emphasis on less proxy normal deviation. Figure 8 also shows the amount of final proxies in correspondence to the chosen value of η . It is not surprising that with a decreasing number of η , the number of proxies increases as this decreases the error measure (5) in order to meet the prescribed threshold. Note further that the resulting meshes contain vertices where more than three proxies meet, see the fourth and fifth column in Figure 8. While it is not problematic in this case, it does cause problems for a different model, see Section 6.2.3.

6.2.2. Face Reconstruction on the Fandisk Model

We proceed to discuss a more involved geometry, namely the Fandisk model (CAD) with $\aleph = 38,840$ vertices, shown in Figure 9. Here, we started the segmentation with 36 manually selected seeds, $\eta = 75$, and without using splits or merges. We consequently obtained $m = 36$ proxy regions, shown in Figure 9a.

Reconstructing this model is challenging to our algorithm in two aspects. First, our simplification procedure requires star-convex faces, see Section 5.2. However, the orange front plate of the fandisk model is not star-convex with respect to its barycenter (Figure 5b, bottom) and thus a first automatic reconstruction is slightly faulty (Figure 9b). These errors are easily identified and fixed by assigning a correct order to the contributing face vertices. See Section 7 for a discussion how to circumvent the requirement of star-convex proxies. The second challenging aspect is caused by the sensitivity of neighborhood notions for different densities in the point set. For example, the light-purple region fits between the blue and purple and hence, they see each other (Figure 9c, right marked spot). However, their planes are almost parallel, and so their intersection appears as an outlier. This could be avoided, if we forbid intersection points built by almost parallel planes or if we for-

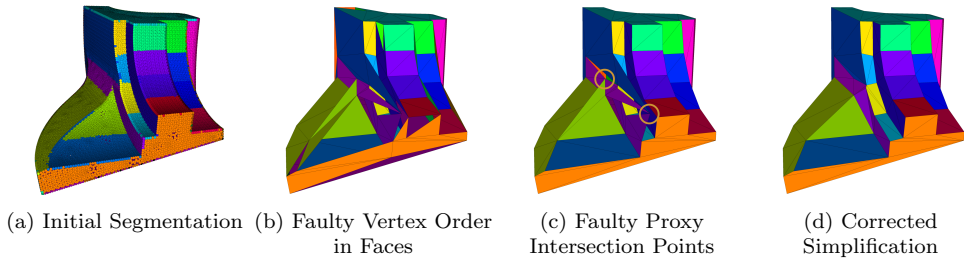


Figure 9: Segmentation and simplification (plane intersection) of the Fandisk model.

bid those intersections that lie too far away from either one of the proxies. The behavior of a misplaced intersection point is also the case for the one produced by the light green, light purple and purple proxies (Figure 9b left marked spot), whereas in consequence a gap results between the light purple and blue area, which should not be there, according to the segmentation. As before, we manually removed faulty intersection points and reset face incidences to obtain a clean mesh for visual representation (Figure 9d).

Note that these challenges are unique to the setting of point sets. In the context of meshed geometries, the intersection vertices can simply be ordered along the boundary of their respective proxy region, yielding a feasible face. Also, neighborhood relations in the mesh setting can be computed via shared edges and do not require an additional neighborhood parameter k . Hence, the works of Cohen-Steiner et al. (2004); Yan et al. (2006) did not have to tackle these issues, while the work of Lee and Bo (2016) does not contain any description of how they solved these problems.

6.2.3. Robustness against Noise on the Dodecahedron Model

As our final experiment, we consider the simplification of a dodecahedron equipped with Gaussian noise in normal direction with an amplitude of 25% of the average neighbor distance (taken as averaged sum over all points and their 12 nearest neighbors.). This geometry is not easily translated into a clean mesh and therefore, the methods of Cohen-Steiner et al. (2004); Yan et al. (2006) cannot be applied here straightforward. The model consists of $\aleph = 962$ and we started with 12 randomly chosen seeds and a threshold of $\eta = 50$. Here, in contrast to the other experiments, we use a neighborhood size of $k = 12$, because of the involved noise components. The otherwise used value of $k = 8$ caused points to not be associated to any proxies. Furthermore, we allowed for splits and merges. The algorithm converged after 8

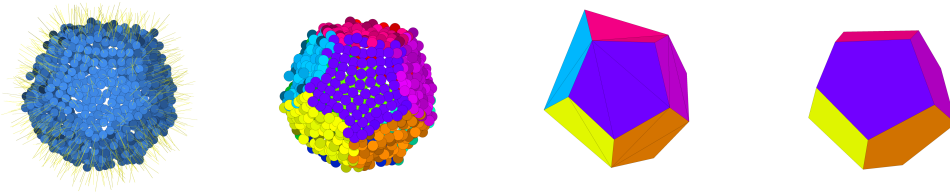


Figure 10: Noisy Dodecahedron, its segmentation and simplifications (planar intersection and optimization).

iterations with $m = 11$ final proxies, see Figure 10. Observe that the faces reflecting the top proxy in the third image are not planar, which is a possible occurrence outlined in the intersection of planes when finding the simplified mesh vertices. In contrast, the optimization provides planar patches (right-most image).

The segmentation reflects the different parts of the geometry correctly. This probably results from the normal differences caused by the noise still being smaller than the normal differences between the different faces of the dodecahedron. Hence, if the noise level and its influence in normal deviation still lies beyond the normal deviation of neighboring geometry regions, its segmentation will reflect the geometric structure well. However, this still depends on initial seed placements and therefore also on performing splits and merges.

With a segmentation reflecting the correct structure of the geometry, the simplification should not cause any additional issues, as it is the result of proxy plane intersections. Only the neighborhood relation between proxies might be more involved, as point locations now deviate more because of additional noise components.

7. Conclusion and Further Research

We have shown in this paper that variational shape approximation is an effective approach to obtain a simplified mesh not only from meshed input, but also from geometries sampled by point sets. The presented example for non-convergence of the VSA method as used in Cohen-Steiner et al. (2004); Yan et al. (2006); Lee and Bo (2016) was successfully circumvented by the introduction of a new *switch* operation for which we proved convergence. Furthermore, by two more operations in the pipeline, namely *split* and *merge*, we eliminate the dependency of both the number and placement of initial seed

points. Finally, we give a detailed description on how to obtain a simplified mesh from the segmented point set by building on the method of tangent plane intersection. Several directions are left for further research.

First, on a theoretical level, we have shown that the introduction of the *switch* operation results in guaranteed convergence. However, it remains unclear whether other alterations of the pipeline exist that came with the same result and do not affect the runtime of the algorithm as heavily as the *switch* operation does.

Second, concerning the parameters, we currently do not provide any theoretical reasons for the choice of weights ω_j in Equation (4) or weights \tilde{w}_j in Equation (8). A better understanding of these weights, aside from the experimental values used in the paper, is desirable. Similarly, the sum of normal differences η is not directly related to the curvature of a proxy, as it depends on the number of points contributing to the sum. Here, a threshold should be found that is independent of the number of points.

Third, our simplification process can currently not handle planar patches which are not star convex. An idea is to include border-detection algorithms for point sets to find both outer and possible inner borders—resulting from holes—of the points associated to the proxy. Given these, the mesh vertices can be easily sorted and a planar face can be obtained while not covering the holes.

Fourth and finally, we have presented an experiment on a noisy point set. We assume that the treatment of meshes equipped with noise should be equally possible and yield even better results because of the explicit connectivity. To investigate this behavior is also left as future work.

Acknowledgments

This research was supported by the DFG Collaborative Research Center TRR 109, “Discretization in Geometry and Dynamics”, the BMS, ECMATH, and the German National Academic Foundation.

The authors would like to thank the anonymous reviewers for their comments which lead to a significant improvement of the paper.

Appendix A. Interpretation of parameter η

In Section 4.3, we introduced the user-chosen parameter η . It relates to the energy $\mathcal{L}^{2,1}$ as presented in Equation (4). From the definition of $\mathcal{L}^{2,1}$, it

is clear that two factors contribute to the value $\mathcal{L}^{2,1}(P_i, N_i)$ a given proxy P_i can achieve. These are:

- The number of points p_j assigned to the proxy and
- the Euclidean distance of the proxy normal N_i to the respective point normals n_j .

That is, a proxy can achieve a low energy by either exhibiting low deviation in its normals or by containing a low number of points. In particular the latter aspect highly depends on the number of points and the point densities in the considered model. Therefore, no general values of η can be presented in this paper, but the user has to choose an appropriate value for the given setup. In the following, we present a simple heuristic how to make an (initial) choice for η .

Any point on a smooth surface can be approximated via a quadric, i.e. a (hyperbolic) paraboloid Dai and Newman (1998). As we handle mostly (locally) convex objects, we consider an elliptic paraboloid as a simple model for a curved surface, parameterized as

$$\mathcal{P} = \left(u, v, \frac{u^2}{a^2} + \frac{v^2}{b^2}\right),$$

then it has mean curvature

$$H(u, v) = \frac{a^2 + b^2 + \frac{4u^2}{a^2} + \frac{4v^2}{b^2}}{a^2b^2\sqrt{\left(1 + \frac{4u^2}{a^4} + \frac{4v^2}{b^4}\right)^3}}. \quad (\text{A.1})$$

A normal to \mathcal{P} at (u, v) is given as

$$\mathcal{P}_u \times \mathcal{P}_v = \begin{pmatrix} 1 \\ 0 \\ 2u/a^2 \end{pmatrix} \times \begin{pmatrix} 0 \\ 1 \\ 2v/b^2 \end{pmatrix} = \begin{pmatrix} -2u/a^2 \\ -2v/b^2 \\ 1 \end{pmatrix}.$$

Hence, after normalization, the point parameterized at (u, v) contributes the following value to $\mathcal{L}^{2,1}$, when assuming that the points are distributed uniformly on the paraboloid and therefore the proxy normal is just $N_i = (0, 0, 1)^T$:

$$\begin{aligned} & \left\| \frac{1}{\sqrt{4u^2/a^4 + 4v^2/b^4 + 1}} \begin{pmatrix} -2u/a^2 \\ -2v/b^2 \\ 1 \end{pmatrix} - \begin{pmatrix} 0 \\ 0 \\ 1 \end{pmatrix} \right\|^2 \\ &= 2 - \frac{2}{\sqrt{4u^2/a^4 + 4v^2/b^4 + 1}}. \end{aligned}$$

Placing a number \aleph_i of points regularly on the domain $[-1, 1] \times [-1, 1]$, i.e. choosing $u = j/\nu_i, v = \ell/\nu_i$ for $j, \ell = 1, \dots, \nu_i$ and $\nu_i := \lceil \frac{\sqrt{\aleph_i}-1}{2} \rceil$, we can compute the total value of $\mathcal{L}^{2,1}$ for these points, depending on the curvature prescribed by (a, b) as

$$\mathcal{L}^{2,1}(P_i, N_i) = 2(2\nu_i + 1)^2 - \sum_{j=-\nu_i}^{\nu_i} \sum_{\ell=-\nu_i}^{\nu_i} \frac{1}{\sqrt{\left(\frac{j}{\nu_i a^2}\right)^2 + \left(\frac{\ell}{\nu_i b^2}\right)^2 + \frac{1}{4}}}. \quad (\text{A.2})$$

Now Equation (A.2) provides a heuristic to compute an (initial) value of η : A user of the algorithm first chooses a desired curvature, to be covered by the proxies. From this choice and a distribution on the two main curvature directions, via Equation (A.1), the parameters (a, b) can be computed. As the user also knows the models to which the algorithm will be applied and therefore the resolution, i.e. the number of points to be included, a second choice is the number of points \aleph_i that is roughly to be covered by a single proxy. From these two choices, using Equation (A.2), a first estimate for η can be computed. If the output of the algorithm is not satisfactory, the user is of course free to tune the parameter towards the desired result.

References

- Attene, M., Patanè, G., 2010. Hierarchical structure recovery of point-sampled surfaces, in: *Computer Graphics Forum*, Wiley Online Library. pp. 1905–1920.
- Berger, M., Tagliasacchi, A., Seversky, L.M., Alliez, P., Guennebaud, G., Levine, J.A., Sharf, A., Silva, C.T., 2017. A survey of surface reconstruction from point clouds. *Comput. Graph. Forum* 36 (1), pp. 301–329.
- Cohen-Steiner, D., Alliez, P., Desbrun, M., 2004. Variational Shape Approximation, in: *ACM Transactions on Graphics (TOG)*, ACM. pp. 905–914.
- Cutler, B., Whiting, E., 2007. Constrained planar remeshing for architecture, in: *Proceedings of Graphics Interface 2007*, pp. 11–18.
- Dai, M., Newman, T.S., 1998. Hyperbolic and parabolic quadric surface fitting algorithms—Comparison between the least squares approach and the parameter optimization approach. Technical Report. University of Alabama.

- Garland, M., Heckbert, P.S., 1997. Surface simplification using quadric error metrics, in: Proceedings of the 24th annual conference on Computer graphics and interactive techniques, pp. 209–216.
- Grilli, E., Menna, F., Remondino, F., 2017. A review of point clouds segmentation and classification algorithms. The International Archives of Photogrammetry, Remote Sensing and Spatial Information Sciences XLII-2 (W3), 339–344.
- Harris, P., Brunson, C., Charlton, M., 2011. Geographically weighted principal components analysis. International Journal of Geographical Information Science 25, pp. 1717–1736.
- Hu, Y., Zhou, Q., Gao, X., Jacobson, A., Zorin, D., Panozzo, D., 2018. Tetrahedral meshing in the wild. ACM Trans. Graph. 37, 60–1.
- Hua, Z., Huang, Z., Li, J., 2015. Mesh simplification using vertex clustering based on principal curvature. International Journal of Multimedia and Ubiquitous Engineering 10, pp. 99–110.
- Lee, K.W., Bo, P., 2016. Feature curve extraction from point clouds via developable strip intersection. Journal of Computational Design and Engineering 3, pp. 102–111.
- Levoy, M., Whitted, T., 1985. The use of points as a display primitive. Technical Report. University of North Carolina, Department of Computer Science. Chapel Hill, NC, USA.
- Lloyd, S.P., 1982. Least squares quantization in pcm. IEEE transactions on information theory 28, pp. 129–137.
- Mathworks, Matlab, . Solve a constrained nonlinear problem, problem-based. URL: <https://www.mathworks.com/help/optim/ug/solve-nonlinear-optimization-problem-based.html>.
- Nguyen, A., Le, B., 2013. 3d point cloud segmentation: A survey, in: 2013 6th IEEE Conference on Robotics, Automation and Mechatronics (RAM), pp. 225–230.
- Pauly, M., Gross, M., Kobbelt, L., 2002. Efficient simplification of point-sampled surfaces, in: Proceedings of the conference on Visualization'02, IEEE Computer Society. pp. 163–170.

- Rabbani, T., Van Den Heuvel, F., Vosselmann, G., 2006. Segmentation of point clouds using smoothness constraint. *International archives of photogrammetry, remote sensing and spatial information sciences* 36, 248–253.
- Rusu, R., Cousins, S., 2011. 3d is here: Point cloud library (pcl), in: *IEEE International Conference on Robotics and Automation (ICRA)*, pp. 6324–6328. doi:10.1109/ICRA.2011.5980567.
- Schnabel, R., Wahl, R., Klein, R., 2007. Efficient ransac for point-cloud shape detection, in: *Computer graphics forum*, Wiley Online Library. pp. 214–226.
- Skrodzki, M., 2019. Neighborhood Data Structures, Manifold Properties, and Processing of Point Set Surfaces. Ph.D. thesis. Freie Universität Berlin. Berlin, Germany. URL: <https://refubium.fu-berlin.de/handle/fub188/25320>.
- Skrodzki, M., Jansen, J., Polthier, K., 2018. Directional density measure to intrinsically estimate and counteract non-uniformity in point clouds. *Computer Aided Geometric Design* 64, 73–89.
- Skrodzki, M., Zimmermann, E., Polthier, K., 2019. Variational Shape Approximation of Point Set Surfaces, in: *IGS 2019 International Geometry Summit – Poster Proceedings*, pp. 54–57.
- Sosorbaram, B., Fujimoto, T., Chiba, N., 2010. Simplification of point set surfaces using bilateral filter and multi-sized splats. *The Journal of the Society for Art and Science* 9 (3), pp. 140–153.
- Wu, J., Kobbelt, L., 2005. Structure recovery via hybrid variational surface approximation, in: *Computer Graphics Forum*, Wiley Online Library. pp. 277–284.
- Xie, Y., Tian, J., Zhu, X.X., 2019. A review of point cloud semantic segmentation. *arXiv:1908.08854*.
- Yan, D.M., Liu, Y., Wang, W., 2006. Quadric surface extraction by variational shape approximation, in: Kim, M.S., Shimada, K. (Eds.), *Geometric Modeling and Processing - GMP 2006*, Springer Berlin Heidelberg, Berlin, Heidelberg. pp. 73–86.

- Yao, L., Huang, S., Xu, H., Li, P., 2015. Quadratic error metric mesh simplification algorithm based on discrete curvature. *Mathematical Problems in Engineering* 2015.
- Zimmer, H., Campen, M., Herkrath, R., Kobbelt, L., 2012. Variational tangent plane intersection for planar polygonal meshing, in: Hesselgren, L., Sharma, S., Wallner, J., Baldassini, N., Bompas, P., Raynaud, J. (Eds.), *Advances in Architectural Geometry 2012*. Springer, pp. 319–332.